Efficient Intracellular Delivery of Molecules with High Cell Viability Using Nanosecond-Pulsed Laser-Activated Carbon Nanoparticles

Aritra Sengupta,[†] Sean C. Kelly,[‡] Nishant Dwivedi,[‡,§] Naresh Thadhani,[‡] and Mark R. Prausnitz[†,*]

[†]School of Chemical and Biomolecular Engineering, Georgia Institute of Technology, Atlanta, Georgia 30332, United States, [‡]School of Materials Science and Engineering, Georgia Institute of Technology, Atlanta, Georgia 30332, United States, and [§]School of Medicine, Boston University, Boston, Massachusetts 02118, United States

ABSTRACT Conventional physical and chemical methods that efficiently deliver molecules into cells are often associated with low cell viability. In this study, we evaluated the cellular effects of carbon nanoparticles believed to emit photoacoustic waves due to nanosecond-pulse laser activation to test the hypothesis that this method could achieve efficient intracellular delivery while maintaining high cell viability. Suspensions of DU145 human prostate carcinoma cells, carbon black (CB) nanoparticles, and calcein were exposed to 5—9 ns long laser pulses of near-infrared (1064 nm wavelength) light and then analyzed by flow cytometry for intracellular uptake of calcein and cell viability by propidium iodide staining. We found that intracellular uptake increased and in some cases saturated at high levels with only small losses in cell viability as a result of increasing laser fluence, laser exposure time, and as a unifying parameter, the total laser energy. Changing interpulse spacing between 0.1 and 10 s intervals showed no significant change in bioeffects, suggesting that the effects of each pulse were independent when spaced by at least 0.1 s intervals. Pretreatment of CB nanoparticles to intense laser exposure followed by mixing with cells also had no significant effect on uptake or viability. Similar uptake and viability were seen when CB nanoparticles were substituted with India ink, when DU145 cells were substituted with H9c2 rat cardiomyoblast cells, and when calcein was substituted with FITC-dextran. The best laser exposure conditions tested led to 88% of cells with intracellular uptake and close to 100% viability, indicating that nanosecond-pulse laser-activated carbon nanoparticles can achieve efficient intracellular delivery while maintaining high cell viability.

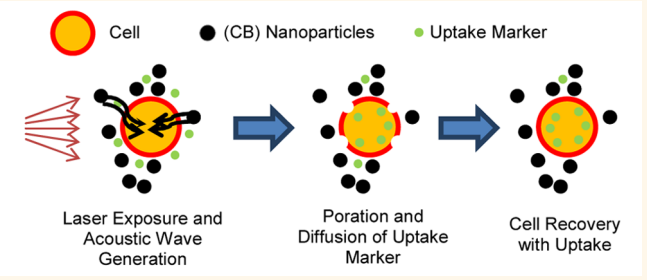

KEYWORDS: carbon black nanoparticles · intracellular drug delivery · near-infrared laser

Many pharmaceutical agents in development and used clinically need to be delivered intracellularly to have their intended therapeutic effect.[1] Inside the cell they have various targets, including nuclear targets for gene transfection, gene correction and other gene-based therapies;[2] mitochondrial targets for certain proapoptotic drugs;[3,4] and other cytoplasmic sites, including those needed for protein knockdown by RNA interference using siRNA or miRNA.[5]

However, the highly structured and lipophilic nature of the cells' plasma membranes generally blocks the direct intracellular delivery of such compounds, such that most molecules other than small ions enter cells by an active transport mechanism, such as receptor-mediated endocytosis.[6] Uptake *via* that route can be accessed through the use of lipid and polymer nanoparticles, especially if decorated with receptor-targeted ligands.[7] However, such chemical delivery systems can be associated with cytotoxicity and drugs administered by that route can be subject to lysosomal degradation after internalization.[8] Viral vectors also harness natural mechanisms of intracellular delivery, but are primarily useful only for DNA delivery and suffer from risks of virus-induced toxicity.[9]

Another approach to intracellular delivery uses physical forces to transiently and reversibly disrupt the cell membrane,

* Address correspondence to prausnitz@gatech.edu.

Received for review January 7, 2014 and accepted February 10, 2014.

Published online February 18, 2014
10.1021/nn500100x

thereby allowing molecules to directly enter the cytoplasm of cells either by diffusion or, in some cases, by electrophoretically driven processes through short-lived transmembrane pores.[10] Examples of such methods are electroporation,[11] ultrasound-mediated intracellular delivery[12,13] and microinjection.[14] Some methods of intracellular delivery have used lasers, for example, to generate acoustic waves from a shock tube to induce uptake by a mechanical mechanism,[15,16] to heat nanoparticles to induce uptake by a thermal mechanism,[17−21] to heat nanoparticles for controlled release of encapsulated drugs[22,23] or to heat nanoparticles to cause cell death.[24] A common limitation of intracellular delivery methods is a trade-off between achieving high levels of intracellular uptake and maintaining high levels of cell viability, since efficient uptake among viable cells is often associated with significant cell death.

In this study, we investigated a method of intracellular delivery that uses laser-activated carbon black (CB) nanoparticles. In this approach, nanosecond pulses from an infrared laser are used to interact with CB nanoparticles, which are believed to emit acoustic waves by a so-called giant photoacoustic effect[25] that mechanically acts on the cell membrane to create transient pores through which molecules can enter the cell. In our previous work, we used a femtosecond laser operating at 810 nm wavelength to demonstrate intracellular delivery by this approach.[26] In the present study, we build off those initial findings in two ways. First, we switched from the expensive and complex femtosecond laser used before to a much simpler and less expensive nanosecond pulse laser. Second, we examine the effects of varying laser exposure conditions over a range of parameters in order to optimize uptake and viability, as well as to gain insight into mechanisms of action.

RESULTS

Intracellular Uptake Due to Laser-Activation of CB Nanoparticles. We first validated that exposure of cells to infrared laser pulses in the presence of CB nanoparticles resulted in uptake of a marker compound, calcein, by viable cells. As shown in Figure 1a, DU145 prostate cancer cells incubated with CB nanoparticles and calcein but, without exposure to laser pulses, did not show significant intracellular uptake of calcein. This treatment is referred to here as a "sham" exposure, where cell samples received the same treatment as laser-exposed samples, except the laser was not activated. In Figure 1b, cells were exposed to laser pulses, but there were no CB nanoparticles present. Again, insignificant uptake was seen.

In contrast, Figure 1c shows the effects of pulsing with a laser in the presence of CB nanoparticles, where the majority of cells appear green, indicating intracellular uptake of green-fluorescent calcein.

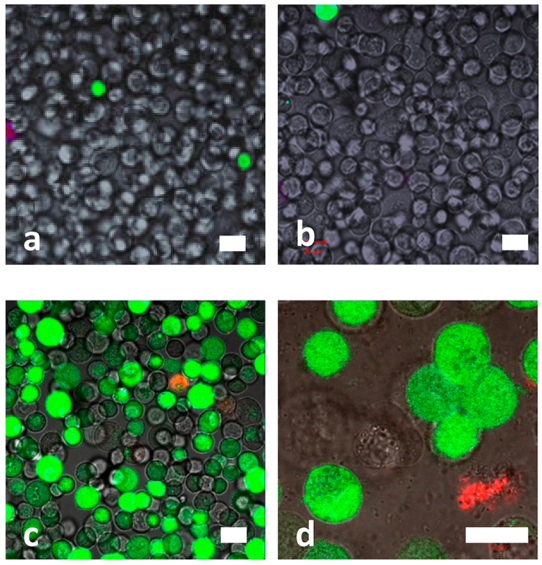

Figure 1. Fluorescence imaging of intracellular uptake. Cells inspected visually using a confocal microscope show that there is little uptake of calcein (green) when cells were exposed to just carbon black (CB) nanoparticles but no laser (a), very little uptake when cells were exposed to laser but not CB nanoparticles (b), and extensive uptake when cells were exposed to laser with CB nanoparticles at 44 mJ/cm^2 fluence, 1 min exposure time, 10 Hz pulsing frequency and 21.4 mm beam diameter (c). Closer inspection of these cells at higher magnification reveals that calcein is present throughout the interior of the cells and not just localized, for example, to endosomes (d). In all samples, very few cells were stained with propidium iodide (red), which is a marker of necrotic and late apoptotic deaths. Scale bars are 20 μm.

Finally, Figure 1d shows a magnified view of cells exposed to laser pulses and CB nanoparticles, further indicating that the calcein is located throughout the interior of the cells rather than, for example, being sequestered in endosomal vesicles.

Effects of Laser Pulse Fluence, Number of Pulses, Beam Spot Size, and Pulse Repetition Rate on Intracellular Uptake and Cell Viability. We next quantified intracellular uptake of calcein and viability in DU145 cells as a function of laser fluence, while keeping all other exposure parameters constant (Figure 2). The time of exposure was set to 1 min at 10 Hz pulsing frequency. Laser exposure at the lowest fluence studied (12.5 mJ/cm^2 per pulse) caused no significant uptake or viability loss compared to the "sham" negative control (Figure 2a). As laser fluence increased, intracellular uptake increased as well, climbing from 30% of cells with uptake at a fluence of 18.75 mJ/cm^2 to 76% of cells with uptake at a fluence of 44 mJ/cm^2 (ANOVA, $p < 0.0001$). Above 44 mJ/cm^2, intracellular uptake no longer increased and maintained a value of approximately 70−80% of the cells (ANOVA, $p = 0.98$) with uptake. Over the full range of laser fluence conditions studied, the viability remained insignificantly different from sham control samples in almost all cases (ANOVA, $p = 0.48$) (Figure 2a).

We expect that laser exposure time (*i.e.*, number of laser pulses) would also affect intracellular uptake and

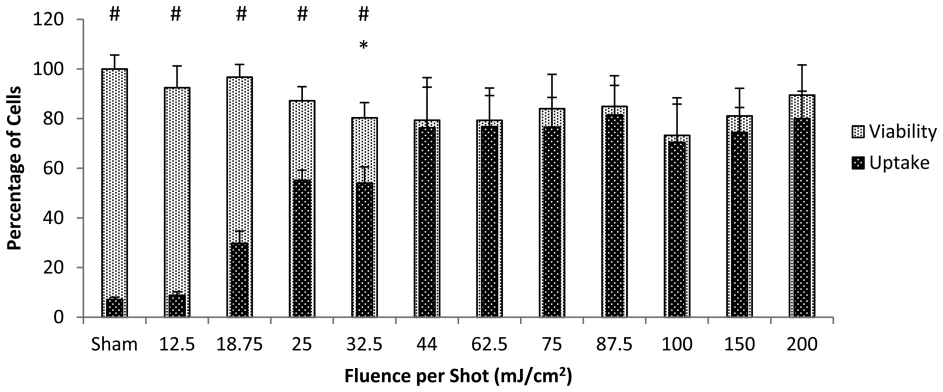

Figure 2. Effect of laser fluence on intracellular uptake and viability of DU145 cells. Cells were exposed to laser for 1 min at various laser fluence levels. Asterisk (*) shows data where viability is lower than sham and hash symbol (#) shows data where uptake is lower than viability ($p < 0.05$). The figure demonstrates saturation of both uptake and viability beyond 44 mJ/cm^2 exposure. All laser exposures were at 10 Hz pulsing frequency and 21.4 mm beam diameter. Data show average ± standard deviation (SD) ($n = 3$ replicates).

viability. Figure 3a,b demonstrates the effect of exposure time on the uptake and viability of DU145 cells, while keeping all the other factors constant. In Figure 3a, the fluence was set to 18.75 mJ/cm^2. The viability did not change significantly compared to sham exposure when the exposure time was increased from 1 to 7 min (ANOVA, $p = 0.97$), whereas the uptake increased from 30% to 88% (ANOVA, $p < 0.0001$). At 7 min, the uptake value was statistically not different from the viability value (Student's *t*-test, $p = 0.36$), indicating that essentially all viable cells had uptake. When the laser fluence was increased to 25 mJ/cm^2 (Figure 3b), there was a decrease in viability as exposure time increased (ANOVA, $p = 0.0014$), and the uptake initially went up and then decreased (ANOVA, $p < 0.0001$). At all times, uptake was significantly less than viability values (Student's *t*-test, $p < 0.05$).

The data on intracellular uptake from Figures 2a and 3a,b are replotted in Figure 3c as a function of total energy input (*i.e.*, pulse fluence × laser beam exposure area × number of pulses). This analysis shows that uptake was proportional to the total energy input below approximately 100 J, which then saturated at a constant uptake value at higher energy inputs.

The data presented so far were generated using a laser beam that fully covered the sample cuvette. When the spot size diameter of the laser beam was reduced from 21.4 mm (full exposure of the cuvette) to 9 mm (16% of the cuvette area was exposed), it resulted in reduced bioeffects. Figure 4a shows that under full cuvette exposure, uptake was higher (Student's *t*-test, $p = 0.002$), but the viability was lower (Student's *t*-test, $p = 0.01$) compared to the partially exposed samples. The total percentage of cells affected by the laser (either uptake or death) was 87% in the case of full cuvette exposure and it was just 40% in the case of 9 mm beam diameter exposure. This value is greater than the 16% of cuvette area, suggesting convection within the cuvette led to more cells entering the laser beam during the exposure time. Additional studies showed that the location of the beam spot in the cuvette did not matter as long as it was within the cuvette area filled with cell solution (data not shown).

The pulsing frequency in the data generated so far was 10 Hz (*i.e.*, 10 pulses per second/s). We therefore also studied slower pulsing frequencies to determine the resulting effect on uptake and viability. Decreasing the pulsing frequency separates each pulse by more time, which means that the cells have more time to recover from the effect of the laser−CB interaction between pulses. In Figure 4b, pulsing frequency was varied between 0.1 and 10 Hz, keeping all the other parameters constant. The viability was unaffected by changing pulsing frequency (ANOVA, $p = 0.35$). The uptake value for 0.1 Hz was a little higher than the rest (ANOVA, $p = 0.025$). This indicates that greater spacing between pulses by decreasing pulsing frequency has little effect on uptake and viability, which further suggests that any recovery by cells after being exposed to a laser pulse and CB interaction processes occurs on a time scale faster than 100 ms (corresponding to 10 Hz pulsing) or possibly slower than 10 s (corresponding to 0.1 Hz pulsing).

Effects of Interaction between Sequential Pulsing Protocols on Uptake and Viability. Our guiding hypothesis is that acoustic energy emitted by CB nanoparticles during laser exposure impacts cells to transiently increase plasma membrane permeability. According to this hypothesis, pretreatment of CB nanoparticles in the absence of cells should have no effect on cells added after the laser exposure. To test this hypothesis, we first exposed cells at a mild laser condition (Figure 5a, condition B) and found that there was no significant change in viability or uptake compared to the sham control (Figure 5a, condition A). In a second experiment, we exposed CB nanoparticles (without cells) to a strong laser condition and then added cells to this

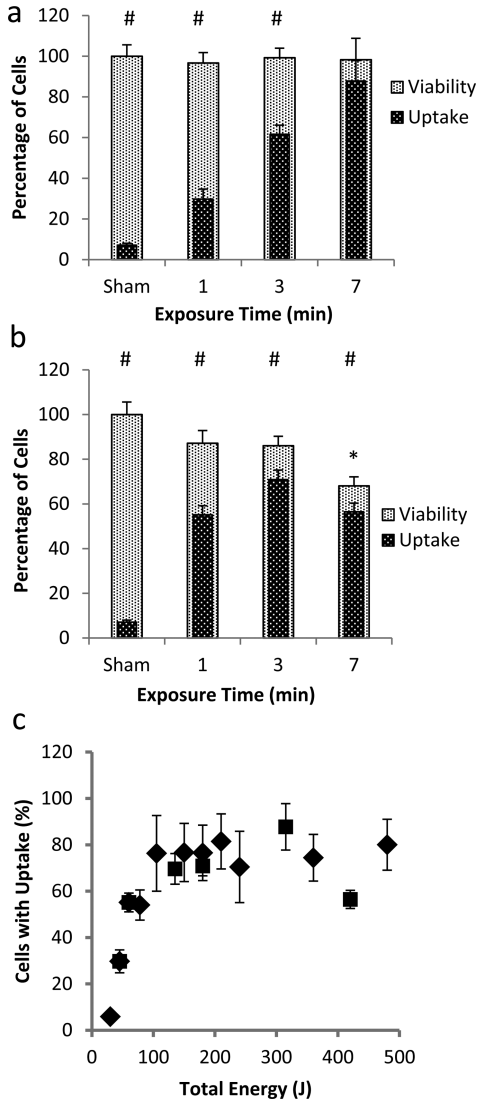

Figure 3. Effect of exposure time and total energy on intracellular uptake and viability of DU145 cells. (a) When fluence was set at 18.75 mJ/cm^2, there was no change of viability, but uptake increased with exposure time until it was the same as viability at 7 min. (b) When fluence was set at 25 mJ/cm^2, viability was less than the sham and uptake was always significantly lower than viability ($p < 0.05$). (c) When total energy is plotted against uptake, at ≥100 J, uptake remained approximately constant at ~75% at higher energy levels. All laser exposures were at 10 Hz pulsing frequency and 21.4 mm beam diameter. Asterisk (*) shows data where viability is lower than sham and hash symbol (#) shows data where uptake is lower than viability. Data show average ± SD ($n = 3$).

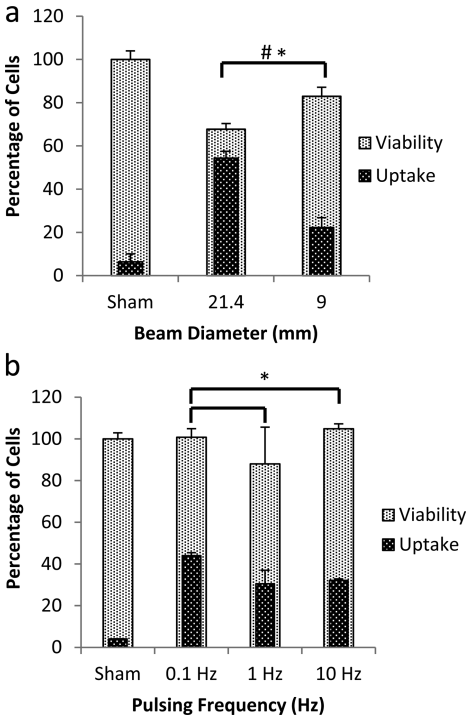

Figure 4. Effect of beam diameter and pulsing frequency on intracellular uptake and viability of DU145 cells. (a) Reducing the beam diameter from 21.4 mm (full cuvette) to 9 mm (16% of the cuvette surface area) resulted in lesser bioeffects, with higher viability and lower uptake (44 mJ/cm^2 fluence, 1 min exposure time, 10 Hz pulsing frequency). (b) Increasing pulsing frequency from 0.1 to 10 Hz while keeping number of pulses at 100 had no statistically significant effect on viability, while uptake was slightly higher at 0.1 Hz compared to 1 and 10 Hz (44 mJ/cm^2 fluence, 21.4 mm beam diameter). Asterisk (*) and hash symbol (#) show statistically significant differences in uptake and viability, respectively ($p < 0.05$). Data show average ± SD ($n = 3$).

solution within 5 s after laser exposure. The resulting solution was then exposed to laser condition B. This effect of CB nanoparticle laser pretreatment (Figure 5a, condition C) had no effect on uptake or viability when compared with condition B (Student's *t*-test, $p = 0.26$). This suggests that cells must be present during laser activation of the CB nanoparticles, because the effects of the activation do not persist after laser exposure.

We next performed an experiment to see if preconditioning cells would have an effect on subsequent laser exposure. We first exposed cells to a mild laser condition, like before, which had no significant effect on viability and minimal effect on uptake (Figure 5b, condition B, Student's *t*-test, $p = 0.26$ for viability and $p = 0.003$ for uptake) and subsequently exposed cells to a moderate laser condition, which significantly increased uptake and decreased viability (Figure 5b, condition D, Student's *t* test, $p = 0.041$ for viability and $p < 0.001$ for uptake). We then combined these two exposures by first exposing cells to the moderate laser condition (thereby preconditioning them) and then exposing the cells to the mild laser condition (Figure 5b, condition E). However, there was no significant difference between conditions D and E (Student's *t*-test, $p = 0.61$ and $p = 0.6$ for viability and uptake, respectively), indicating that preconditioning cells with a moderate exposure did not enhance the effects of a mild exposure. While we examined only one of many possible preconditioning scenarios, the data suggest that the effects of an initial exposure with significant bioeffects do not make cells more susceptible to bioeffects from a subsequent subthreshold exposure. This is consistent with the observation made previously when testing the effects

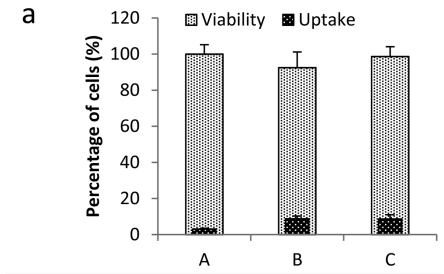

Pretreatment			
Fluence (mJ/cm^2)	-	-	44
Pulses	-	-	1800
Frequency (Hz)	-	-	10
Cell Exposure			
Fluence (mJ/cm^2)	-	12.5	12.5
Pulses	-	600	600
Frequency (Hz)	-	10	10

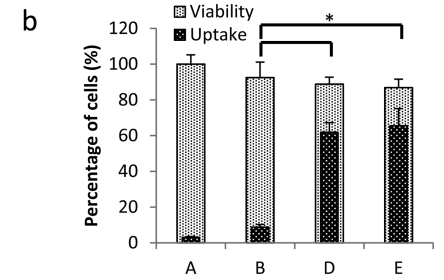

Cell Exposure #1				
Fluence (mJ/cm^2)	-	12.5	44	44
Pulses	-	600	100	100
Frequency (Hz)	-	10	1	1
Cell Exposure #2				
Fluence (mJ/cm^2)	-	-	-	12.5
Pulses	-	-	-	600
Frequency (Hz)	-	-	-	10

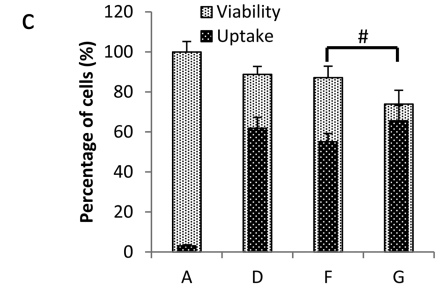

Cell Exposure #1				
Fluence (mJ/cm^2)	-	44	25	44
Pulses	-	100	600	100
Frequency (Hz)	-	1	10	1
Cell Exposure #2				
Fluence (mJ/cm^2)	-	-	-	25
Pulses	-	-	-	600
Frequency (Hz)	-	-	-	10

Figure 5. Effect of pretreatment and sequential laser exposures on intracellular uptake and viability of DU145 cells. (a) Compared to sham treatment (A), there was no significant effect of weak laser exposure of cells in the presence of CB nanoparticles (B). Very strong laser exposure of CB nanoparticles (without cells) as a pretreatment followed by addition of cells and weak laser exposure (C) was not significantly different from conditions (B) and (A) in terms of uptake and viability. (b) The sequential combination of a strong laser exposure and weak laser exposure (E) was statistically no different from the strong laser exposure alone (D) and much greater than the weak laser exposure alone (B) in terms of uptake and viability. (c) The sequential combination of two strong laser exposures with different laser parameters (G) had lower viability but uptake was not statistically different from either of the individual laser exposures alone (D, F). All laser exposures were at 10 Hz pulsing frequency and 21.4 mm beam diameter. Asterisk (*) and hash symbol (#) show statistically significant differences in uptake and viability, respectively ($p < 0.05$). Data show average ± SD ($n = 3$).

of pulsing frequency (Figure 4b), which indicated that cells do not appear to have a "memory" of previous exposures if the exposures are spaced by >100 ms.

Another combination of laser CB interaction was examined employing moderate laser conditions. One exposure involved stronger fluence and shorter exposure time, while the other exposure involved weaker fluence and longer exposure time. We found that each condition by itself increased uptake and decreased viability (Figure 5c, conditions D and F, Student's *t*-test, $p = 0.044$ and $p < 0.001$ for viability and uptake, respectively, for condition F). The combination of applying condition D followed by condition F within 5 s led to a significant decrease in viability (Student's *t*-test, $p = 0.03$) with no significant change in uptake (Student's *t*-test, $p = 0.53$) (Figure 5c, condition G). The viability in condition G (*i.e.*, 74%) was roughly the product of the viability in conditions D and F (88% × 87% = 76%), suggesting an additive, rather than a synergistic effect of this combination. The fact that uptake did not increase further could be explained because the level of uptake was statistically indistinguishable from the level of viability (Student's *t*-test, $p = 0.23$), meaning that essentially all viable cells had uptake.

Effects of CB Nanoparticle Type and Concentration on Uptake and Viability. The proposed mechanism of molecular uptake into cells in this study involves laser energy absorption and transduction by carbon nanoparticles creating photoacoustic effects. Figure 6 shows a comparison between India ink, another form of CB nanoparticle, and CB nanoparticles used so far in this study at various concentrations under the same laser conditions. India ink includes CB nanoparticles as the main component along with other components whose composition are insufficiently characterized.[27,28] We determined by dynamic light scattering, that the mean diameter of particles in India ink was 110 nm (dispersity of 0.23), as compared to 189 nm (dispersity of 0.16) for the CB nanoparticle aggregates. At each condition in the laser exposure experiments, the concentration of India ink particles was adjusted to have the same laser absorption as their CB nanoparticle counterparts.

Considering the effect of nanoparticle concentration first, when CB nanoparticle concentration was increased, keeping all other factors constant, the viability decreased (ANOVA, $p < 0.0001$), which resulted in a decrease of uptake as well (ANOVA, $p < 0.0001$). Under all the exposed conditions, the difference between uptake and viability was statistically nonsignificant (Student's *t*-test, $p > 0.05$). When CB nanoparticles were replaced with India ink particles, there was similarly a decrease in viability (ANOVA, $p < 0.0001$), which again resulted in a decrease in uptake (ANOVA, $p < 0.0001$).

When the effects of the India ink and CB nanoparticles are compared, there is no significant difference at

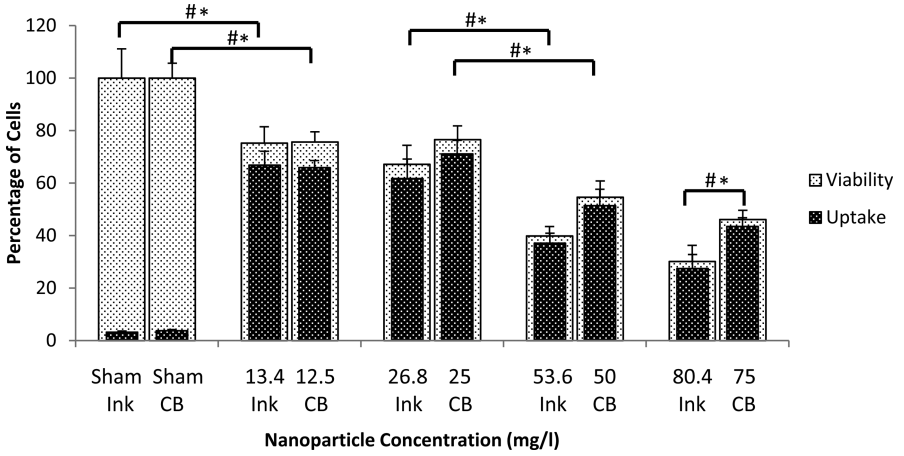

Figure 6. Effect of increasing India ink and CB nanoparticle concentration on intracellular uptake and viability of DU145 cells. In each paired comparison, the concentration of India ink and CB nanoparticles was adjusted so that the laser absorbance was the same. Uptake and viability generally decreased with increasing nanoparticle concentration, and India ink had stronger effects on uptake and viability than CB nanoparticles at the higher concentrations. All laser exposures were at 44 mJ/cm^2 fluence, 1 min exposure time, 10 Hz pulsing frequency and 21.4 mm beam diameter. Asterisk (*) and hash symbol (#) show statistically significant differences in uptake and viability, respectively ($p < 0.05$). Data show average ± SD ($n = 3$).

low particle concentrations (Student's *t*-test, $p > 0.05$), but viability and uptake are both lower in the India ink samples at the highest concentration (Student's *t*-test, $p < 0.05$). Altogether, these results suggest that the specific chemistry of the CB formulation is not as important as the concentration of CB nanoparticles.

Toxicity of CB Nanoparticles. To assess possible toxic effects of the CB nanoparticles, an MTT assay was performed on DU145 cells after exposure to CB nanoparticles at various concentrations for 24 and 72 h. MTT stains cells that are properly respiring, such that lack of staining is an indicator of cytotoxicity. Figure 7 shows the absorbance values as a function of increasing CB nanoparticle concentration. The data were normalized with respect to the CB nanoparticle-free control. There was no significant difference between the absorbance values of the MTT assay at 24 and 72 h (ANOVA, $p = 0.39$). Moreover, there was no significant loss of viability below 200 mg/L (ANOVA, $p = 0.997$ and $p = 0.996$, respectively).

These data produce ED_{50} values of 360 mg/L for the 24 h data and 350 mg/L for the 72 h data. For most experiments in this study, a CB nanoparticle concentration of 25 mg/L was used, which is an order of magnitude lower than the ED_{50} value. Visual inspection of cells incubated with high-concentration CB nanoparticles showed the particles coating the cell surface (data not shown). This steric interaction, rather than a chemical interaction, might have affected cell viability at the higher concentrations. The analysis indicates that at the concentrations used in this study, there was no significant change to cell viability as a result of extended exposure to CB nanoparticles.

Effects of Cell Type and Molecular Weight of Uptake Marker on Uptake and Viability. In addition to DU145 prostate cancer cells, we also studied the effects of

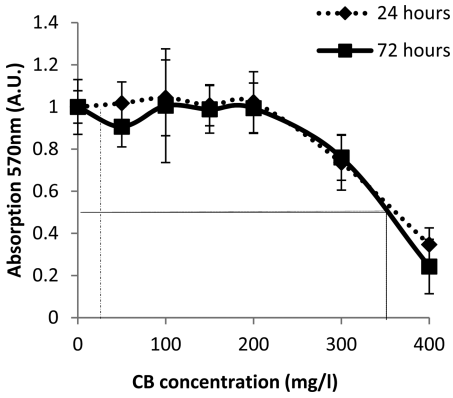

Figure 7. Toxicity of CB nanoparticles on DU145 cells measured by MTT cytotoxicity assay. Cells were exposed to CB nanoparticles for 24 and 72 h, which yielded ED_{50} values of 350 and 360 mg/L, respectively. These values are ~14 times higher than the concentration (25 mg/L) used in most experiments in this study. Data show average ± SD ($n = 3$).

laser-activated CB nanoparticles on H9c2 rat cardiomyoblasts. The experiments with these cells were performed at exposures of 25 mJ/cm^2 for 1 and 3 min, keeping all other parameters constant (Figure 8). When the performance of the two cell lines was compared, the viability was statistically not different from each other (ANOVA, $p = 0.94$), but the uptake was lower for H9c2 cells (ANOVA, $p = 0.007$). These data show that the effects of laser-activated CB nanoparticles on cell uptake and viability are seen in multiple cell types.

The delivery efficiency was also characterized by varying the molecular weight of the uptake markers (Figure 9). Calcein was replaced with FITC-labeled dextrans of molecular weights 10, 70, and 500 kDa and exposed to laser at 44 mJ/cm^2 for 1 min, keeping all other parameters constant. There was no statistical difference between the viability of the exposed

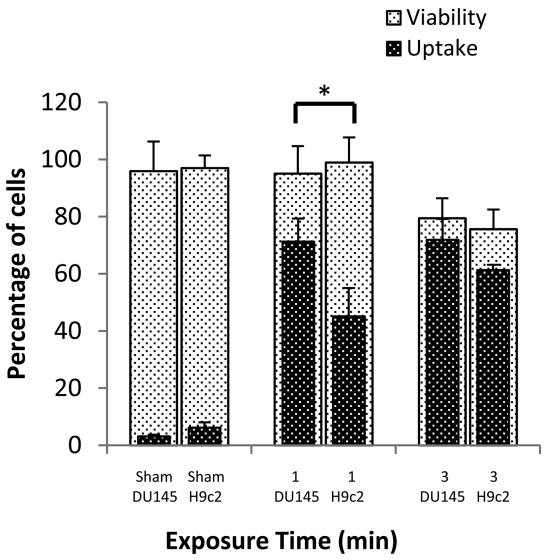

Figure 8. Comparison of intracellular uptake and viability of two cell lines (DU145 and H9c2) after the same laser exposures. Cell viability was the same, whereas uptake after the 1 min exposure was significantly different between the two cell lines. All laser exposures were at 25 mJ/cm^2 fluence, 10 Hz pulsing frequency and 21.4 mm beam diameter. Asterisk (*) shows statistically significant difference in uptake ($p < 0.05$). Data show average ± SD ($n = 3$).

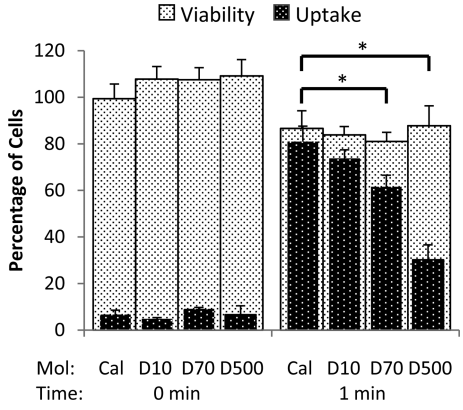

Figure 9. Effect of molecular weight on intracellular uptake and viability after the same laser exposures. There is no statistical difference in viability across all samples, whereas the uptake decreased as the molecular weight was increased for calcein (Cal), 10 kDa dextran (D10), 70 kDa dextran (D70), and 500 kDa dextran (D500). All laser exposures were at 44 mJ/cm^2, 10 Hz and 21.4 mm beam diameter. Asterisk (*) shows statistically significant difference in uptake ($p < 0.05$). Data shows average ± SD ($n = 3$).

samples (ANOVA, $p = 0.92$), whereas uptake decreased with increasing molecular weight (ANOVA, $p = 0.022$).

Trade-Off between Maximizing Uptake and Maximizing Viability. When mean values of cell viability are plotted against uptake (Figure 10), all data points fall below the viability = uptake line. This is because being counted as an uptake cell requires that the cell must be viable. Some points were at or just below the viability = uptake line, indicating that essentially all viable cells had uptake. No points were at 100% viability and 100% uptake, although we did observe 88% uptake with close to 100% viability.

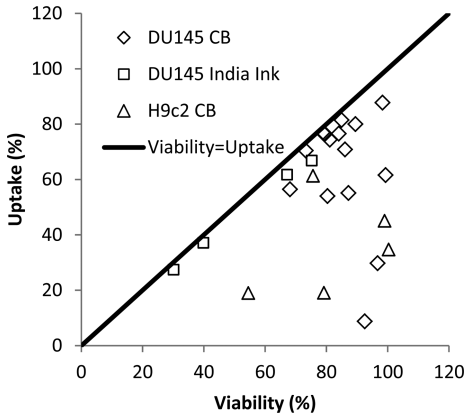

Figure 10. Comparison between intracellular uptake and viability. This graph shows all data generated in this study (*i.e.*, from Figures 2–8). All data points are at or below the uptake = viability line since there cannot be more cells with uptake than cells that are viable.

DISCUSSION

This study was guided by the hypothesis that laser energy is absorbed by CB nanoparticles, which transduce that energy into a form that transiently permeablizes cells, resulting in intracellular uptake and possible loss of cell viability. On the basis of prior literature,[25,26,29] we further believe that the mechanism of energy transduction involves laser–CB nanoparticle interactions leading to the sudden heating of the nanoparticles, which leads to generation of acoustic emissions (*i.e.*, pressure waves) caused by thermal expansion of the nanoparticles, as well as possibly the vaporization of water and/or chemical reaction between water and carbon (*i.e.*, $C(s) + H_2O(l) \rightarrow CO(g) + H_2(g)$). Elucidating the details of this energy transduction mechanism is beyond the scope of this study.

There should be two time scales associated with this process. The first time scale is that of laser absorption by CB nanoparticles followed by pressure wave generation. The second time scale is that of cell membrane permeablization, intracellular uptake and membrane resealing. We expect that the time scale of the first step is at least nanoseconds (*i.e.*, the time scale of the laser pulse), but may be longer, given the time it may take to grow and collapse gas bubbles, if they are involved in the mechanism.[30] The time scale associated with intracellular uptake through permeablized membranes is likely much longer, given that it involves transmembrane diffusion and cell membrane resealing mechanisms.

In general, we would expect that more energy transduction from laser irradiation to acoustic emissions should increase bioeffects on cells. Thus, increased energy transduction should be associated with both increased intracellular uptake as well as increased loss of cell viability. Because of this, the goal for applications

is to find conditions that optimize uptake without significant loss of viability. The present study showed that increasing fluence and number of laser pulses (*i.e.*, time of irradiation), both increased energy input and, therefore, increased energy output to cells. Increasing CB nanoparticle concentration increased the number of acoustic sources and thereby increased energy output to cells without increasing energy input. Consistent with our hypothesis, increasing each of these three parameters led to increased uptake and loss of viability, depending on the details of the exposure conditions. The optimal conditions found in this study involved 18.75 mJ/cm^2 laser fluence, 7 min exposure of DU145 cells with 25 mg/L CB nanoparticle concentration, and thereby achieving an intracellular delivery efficiency of 88% with 98% viability (Figure 3a).

There was no significant effect on uptake or viability due to laser exposure alone (Figure 1a), incubation with CB nanoparticles alone ("sham" experiments), or pretreatment of CB nanoparticles with a strong laser exposure (Figure 5a), which is also consistent with the mechanism involving laser energy transduction by CB nanoparticles. Increasing laser fluence initially increased uptake, but then the effects of increasing fluence saturated, which produced cells with efficient uptake and little loss of viability (Figure 2). In contrast, increasing the duration of the laser exposure increased uptake until the point where it started killing cells (Figure 3b). This suggests that the effect of increasing the "force" applied to cells saturates whereas increasing the time over which that force acts on the cells does not. This interesting relationship is similar to previous observations in electroporation-mediated uptake, where the effects of increasing voltage resulted in saturated uptake, but the effects of increasing number or length of electrical pulses did not.[31]

At the conditions used in this study, increasing the concentration of CB nanoparticles increased bioeffects in the form of killing more cells. We did not see an increase in uptake, because, at the lower CB nanoparticle concentration used, almost all viable cells already had uptake. Thus, we saw a decrease in uptake due to cell death. At the lowest CB nanoparticle concentration studied (12.5 mg/L), the nanoparticle-to-cell ratio was approximately 100:1, whereas at the highest concentration (75 mg/L), it was approximately 600:1. In general, more acoustic emission sites should produce more pressure waves impacting cells. However, the details of this interpretation are complicated by constructive and destructive interference of waves in the complex acoustic field.

Uptake and viability did not depend strongly on pulsing frequency of the laser (Figure 4b). This suggests either that each pulse creates independent effects on the cells, which would mean that the time scale for onset and reversal of the direct bioeffects of the laser exposure is shorter than 100 ms (corresponding to pulsing at a frequency of 10 Hz) or possibly that the time scale is much longer than 10 s (corresponding to pulsing at a frequency of 0.1 Hz), such that interacting effects of each pulse on the next one(s) are not affected by changing their separation from 0.1 to 10 s. Given the nanosecond time scale of the laser exposure itself, we hypothesize that the first scenario above is the more likely scenario, such that intracellular uptake and bioeffects that initiate loss of viability occur on a time scale shorter than 100 ms. Our interpretation is further supported by the data in Figure 5b, which showed that pretreatment of cells with a moderate laser condition did not make them more susceptible to subsequent exposure to mild laser conditions a few seconds later.

When CB nanoparticles were replaced by India ink at concentrations which had the same laser absorbance, the India ink particles were yielded lower viability (Figure 6), which suggests a stronger mechanical effect on the cells. This may be because the nanoparticles in India ink are smaller than CB nanoparticles, which means that for the same mass of carbon, there was a larger number of India ink nanoparticles than CB nanoparticles. An alternative explanation could be that the poorly characterized additional component particles found in India ink might have effects on cells during laser exposure.

Molecules ranging from 0.6 to 500 kDa were delivered into cells, but with decreased efficiency at higher molecular weight. This could be explained by a pore size distribution created in the cell membrane similar in size to that of the molecules, such that the larger molecules were excluded, or at least hindered, by a fraction of the pores. The smallest dextran (10 kDa) has a radius of approximately 2.7 nm and the largest dextran (500 kDa) has a radius of approximately 15 nm,[32] which suggests pores of similar size. Alternatively, decreased uptake of the larger molecules could be explained by their slower diffusion through short-lived membrane pores. According to the Stokes–Einstein equation, the 500 kDa dextran has a diffusivity 5.5 times smaller than that for 10 kDa dextran.

Finally, we can consider future possible applications for targeted intracellular drug delivery guided by this study's findings. Flow cytometry analysis and MTT cytotoxicity analysis suggested that the procedure was well tolerated by cells under the conditions of this study. Similar bioeffects were seen in two cell lines, DU145 human prostate carcinoma cells and H9c2 rat cardiomyocytes, suggesting the generality of the approach to multiple cell types. Uptake was also seen for molecules as big as 500 kDa dextran, although the uptake was significantly reduced at higher molecular weight. Bioeffects were reduced by reducing the beam diameter, which was interpreted to mean that bioeffects were only felt where the laser was focused. This can enable targeting the effects to certain locations.

Altogether, these capabilities suggest an efficient method to load cells with molecules at high cell viability, which can be used for *in vitro* laboratory applications for research or, in the future after additional development, for *in vivo* drug delivery applications in medicine. Some of the advantages of this approach are its relatively simple procedure, the rapid time scale of delivery into cells and the localization of effects at the site of laser focus. A concern is how the nanoparticles of sizes close to 200 nm will be cleared from the tissue after the laser exposure. This approach is mechanistically similar to electroporation and sonoporation, both of which are used clinically,[33,34] but differs in its ability to achieve highly efficient intracellular delivery with high viability using a noninvasive method.

CONCLUSION

This study examined the use of nanosecond laser pulses in the presence of CB nanoparticles to increase intracellular delivery of model compounds, calcein and dextrans, while maintaining high cell viability. We believe that CB nanoparticles absorb the laser energy and transduce it into acoustic outputs that transiently permeablize the cell membranes, although the details of this mechanism are not explored in this study. We found that lower fluence, with lower concentration of CB nanoparticles and longer exposure times, resulted in a "gentler" photoacoustic environment that allowed uptake of molecules in up to 88% of cells with no significant loss of cell viability. Increased fluence or CB nanoparticle concentration was also able to yield high uptake but generally had more cell death. We conclude that the method investigated in this work uses a straightforward protocol to enable efficient intracellular delivery of molecules with high cell viability using nanosecond-pulse laser-activated carbon nanoparticles for laboratory use and possible future *in vivo* applications.

METHODS

Laser Apparatus. The Nd:YAG infrared laser (Powerlite II Plus, Continuum, Santa Clara, CA) available in the High-Strain-Rate Laboratory in the School of Materials Science and Engineering was used to apply pulses of 1064 nm wavelength, 5−9 ns pulse length, and 50−175 mJ energy per pulse. Pulses were applied at a repetition rate of 10 Hz (*i.e.*, 10 pulses/s), unless otherwise stated. In some cases, pulses were applied at 1 or 0.1 Hz. The energy was varied by manipulating the amplifier voltage of the system. The beam was passed through a Faraday isolator to prevent back reflection. The 12 mm-diameter laser beam was passed through a 9 mm-diameter aperture to block the edges of the beam and thereby obtain a more uniform top-hat profile. The resulting 9 mm-diameter beam was then usually diverged to 21.4 mm diameter using a lens to illuminate the entire cuvette (exposure area of 4 cm^2), unless stated otherwise. In some cases, the beam was used directly without diverging (exposure area of 0.63 cm^2). "Sham" exposures were used as negative control experiments, where solutions containing cells, calcein and CB nanoparticles went through all the same steps as exposed samples (see below), except that the laser was not turned on. Another negative control involved only cells without CB nanoparticles or calcein.

Cell Preparation. Human prostate carcinoma cells (DU145, American Type Culture Collection, Manassas, VA) and rat cardiomyoblast cells (H9c2, courtesy of Dr. Mike Davis, Emory University, Atlanta, GA) were cultured as monolayers in a humidified atmosphere of 95% air and 5% CO_2 at 37 °C in RPMI-1640 medium (Cellgro, Herndon, VA) and DMEM (Cellgro), respectively, which was supplemented with 100 g/mL penicillin−streptomycin (Cellgro) and 10% (v/v) heat inactivated FBS (Corning, Palo Alto, CA). For each experiment, cells at 80−90% confluence were harvested by trypsin/EDTA (Cellgro) digestion, washed using fresh growth medium with FBS and resuspended in RPMI at a cell concentration of $\sim 10^6$ cells/mL. The DU145 cells[35] were used as a model cell line in most experiments because they are well characterized and have been used extensively in our previous related studies.[26,36,37] In some experiments, H9c2 cells[38] were used as an alternative model representing a different cell type from a different species.

Nanoparticle Preparation. To prepare the CB nanoparticle solution, 20 mg of CB (Black Pearls 470, Cabot, Boston, MA) was added to 50 mL of 0.013% (v/v) Tween 80 (Sigma-Aldrich, St. Louis, MO; added to reduce aggregation and settling of the nanoparticles) in DI water and sonicated for at least 15 min to obtain the final CB solution at a concentration of 400 mg/L. The size of the individual CB nanoparticles was 25 nm, but they were aggregated into larger particles of 189.3 ± 1.5 nm (n = 3) diameter with a dispersity of 0.16 ± 0.03 (n = 3), as determined from dynamic light scattering measurements. The individual nanoparticles could not be further separated by sonication (neither bath sonicator nor a more powerful needle sonicator). After making the 50 mL solution of CB nanoparticles, it was aliquoted into smaller 1.5 mL samples.

India ink (Chartpak, Leeds, MA), as obtained from the manufacturer, was first diluted to 1% (v/v) in DI water (without surfactant), which served as the stock solution for experiments. Because the manufacturer did not provide technical information about the ink, we dried 1 mL of the India ink solution on wax paper and determined the solids content to be 129 ± 1.45 mg/L (n = 3) by weighing the dried mass. Dynamic light scattering measurements suggested that the mean diameter of the India ink nanoparticles was 110.6 ± 0.74 nm (n = 3) with a dispersity of 0.23 ± 0.01 (n = 3).

Relative absorption by the India ink stock solution was determined by measuring absorption at 1000 nm wavelength and comparing it with the absorption of the CB nanoparticle stock solution of the same volume, which determined that the ratio of the absorption of the India ink stock solution to the CB nanoparticle stock solution was 2.91 ± 0.1 (n = 3). For experiments where India ink and CB nanoparticles were added at the same level of laser absorption, the volume of India ink stock solution added to a sample was 2.91 times less than the volume of CB nanoparticle stock solution.

Sample Exposure. A volume of 520 μL of cells at a concentration of 10^6 cells/mL was suspended in RPMI, transferred to 1.5 mL microcentrifuge tubes and stored on ice until exposure. CB nanoparticle stock solution was added to achieve a final concentration of 25 mg/L CB nanoparticles, unless otherwise noted. In some experiments, different concentrations of CB were used. High purity calcein (Molecular Probes, Eugene, OR) was used as an uptake marker and was added from a stock solution at a final concentration of 10 μM. In some experiments, calcein was replaced by FITC labeled dextrans (Sigma-Aldrich) of 10, 70, and 500 kDa molecular weights at a concentration of 10 μM. The final solution was mixed thoroughly by vortexing and then exposed to laser in cuvettes (37-PX-2, Starna Cuvettes, Santa Clara CA) made from Pyrex glass. The total volume of the cuvette was 600 μL. The top part of the cuvette was cut at 2 mm from the base of the neck to facilitate transfer of liquids. A total volume of 563 μL of the mixture was transferred to the cuvette

using a transfer pipet. The cuvette was placed in a custom-made stand to keep it stationary during laser exposure.

After laser exposure, cells were transferred back to microcentrifuge tubes and stored on ice to reduce uptake due to endocytosis until all the samples were done. Propidium iodide (Invitrogen, Grand Island, NY) was added at a concentration of 7.5 μM and cells were incubated for at least 10 min to label necrotic and late apoptotic cells. Next, cells were centrifuged at 500*g* for 6 min and washed with PBS (Cellgro) supplemented with 10% FBS twice. After the third centrifugation, the cells were suspended in PBS and then transferred to flow cytometer tubes or were put on a microscope slides and coverslipped for fluorescence imaging.

Cytotoxicity of CB Nanoparticles. Dimethyl thiazoldiphenyl tetrazoleum (MTT) assay was performed to assess the cytotoxicity of CB nanoparticles on the cells. CB nanoparticles were added at concentrations ranging from 50 to 400 mg/L to DU145 cells that were monolayer cultured on 96 well plates. The cells were then incubated for either 24 or 72 h with the CB nanoparticles. The cells without CB nanoparticles served as the positive control. The negative control was created by incubating cells with 70% methanol for 30 min. CB nanoparticles were removed from the solution by centrifugation and absorbance measured at 570 nm was used to determine the number of viable cells.

Analysis and Quantification. Cells were imaged using a Zeiss LSM META/NLO 510 multiphoton laser confocal microscope (Zeiss, Thornwood, NY). PMTs, laser power and pinhole aperture were set to minimize bleeding of signal from one dye channel to the other. Images for both the dyes (*i.e.*, calcein and propidium iodide) were taken sequentially to avoid signal overlap. Cells were observed at 20× and 60× magnification to visually inspect cellular uptake in viable cells.

A benchtop flow cytometer (BD LSRII, BD Biosciences, San Jose, CA) was used to quantify uptake, *i.e.*, the number of live cells with calcein uptake, and viability, *i.e.*, the number of live cells that were not necrotic or fragmented, on a cell by cell basis. For quantifying necrotic death, propidium iodide stain was analyzed using a PerCP-Cy5, 670 nm long-pass filter. Calcein uptake into cells was detected using a FITC, 530/28 nm bandpass filter. A cell gate was constructed based on forward-scattered and side-scattered light to determine the size distribution of cells in the control. Any events lying within this gate were considered to be cells, whereas events smaller than that were considered cells fragments. To determine the concentration of intact cells (and thereby account for possible cell loss due to fragmentation), we multiplied the volumetric flow rate in the flow cytometer by the time of analysis to determine the total volume analyzed. Dividing the number of cells detected within the gate by the volume provided the cell concentration, which could be compared to nonexposed controls to determine cell loss due to fragmentation. Approximately 10^5 cell events were collected per sample which was approximately 20% of the total cells present in each sample. To account for spectral overlap between the dyes, compensation controls were run for each experiment. Propidium iodide-positive samples were made by incubating cells in 70% methanol for 30 min and then washing with PBS. Calcein-positive samples were made by exposing cells with CB nanoparticles and calcein at 44 mJ/cm^2 per shot for 3 min. At this condition, there was extensive cell death, but almost all cells which remained viable had calcein uptake.

Statistical Analysis. A minimum of three replicates was performed for all conditions. Replicates enabled calculations of means and standard deviation. The equality of mean response (uptake or viability) between treated samples and sham exposures and other control samples was tested using ANOVA (α = 0.05). To test equality of mean response between pairs of data points, 1-way ANOVA followed by the post hoc Tukey's pairwise comparison was used, whereas 2-way ANOVA was employed to compare three or more data points using Microsoft Excel 2010 (Microsoft, Redmond, WA) and GraphPad Prism 6 (GraphPad Software, La Jolla, CA). The null hypothesis was that the average fraction of cells with uptake (or average fraction of viable cells) between a treated sample and a sham exposure were equal. To compare between mean values of two data points, an unpaired Student's *t*-test, is performed (2 tails) assuming unequal variances.

Conflict of Interest: The authors declare no competing financial interest.

Acknowledgment. We thank P. Joseph and M. Gray for helpful discussions and D. Bondy for providing administrative support. This work was carried out in the Center for Drug Design, Development and Delivery and the Institute for Bioengineering and Bioscience at Georgia Tech, and was supported in part by the National Institutes of Health.

Supporting Information Available: Table listing mean values of uptake and viability of all the data points shown in Figures 1, 2 and 6. This material is available free of charge *via* the Internet at http://pubs.acs.org.

REFERENCES AND NOTES

1. Torchilin, V. P. Recent Approaches to Intracellular Delivery of Drugs and DNA and Organelle Targeting. *Annu. Rev. Biomed. Eng.* **2006**, *8*, 343–375.
2. Templeton, N. S. *Gene and Cell Therapy: Therapeutic Mechanisms and Strategies*, 3rd ed.; CRC Press: Boca Raton, FL, 2008.
3. Yang, A.; Wilson, N. S.; Ashkenazi, A. Proapoptotic DR4 and DR5 Signaling in Cancer Cells: Toward Clinical Translation. *Curr. Opin. Cell Biol.* **2010**, *22*, 837–844.
4. Perez-Pinzon, M. A.; Stetler, R. F.; Fiskum, G. Novel Mitochondrial Targets for Neuroprotection. *J. Cereb. Blood Flow Metab.* **2012**, *32*, 1362–1376.
5. Sioud, M. *siRNA and miRNA Gene Silencing: From Bench to Bedside (Methods in Molecular Biology*; Humana Press: New York, 2009; Vol. 487.
6. Lodhish, H.; Berk, A.; Zipursky, S. L.; Matsudaira, P.; Baltimore, D.; Darnell, J. Receptor-Mediated Endocytosis and the Sorting of Internalized Proteins. In *Molecular Cell Biology*, 4 ed.; W. H. Freeman: New York, 2000.
7. Panyam, J.; Labhasetwar, V. Biodegradable Nanoparticles for Drug and Gene Delivery to Cells and Tissue. *Adv. Drug Delivery Rev.* **2012**, *64* (Supplement), 61–71.
8. Varkouhi, A. K.; Scholte, M.; Storm, G.; Haisma, H. J. Endosomal Escape Pathways for Delivery of Biologicals. *J. Controlled Release* **2011**, *151*, 220–228.
9. Thomas, C. E.; Ehrhardt, A.; Kay, M. A. Progress and Problems with the Use of Viral Vectors for Gene Therapy. *Nat. Rev. Genet.* **2003**, *4*, 346–358.
10. Meacham, J. M.; Durvasula, K.; Degertekin, F. L.; Fedorov, A. G. Physical Methods for Intracellular Delivery: Practical Aspects From Laboratory Use to Industrial-Scale Processing. *J. Lab. Autom.* **2013**, 1–18.
11. Gehl, J. Electroporation: Theory and Methods, Perspectives for Drug Delivery, Gene Therapy and Research. *Acta Physiol. Scand.* **2003**, *177*, 437–447.
12. Liu, Y.; Yan, J.; Prausnitz, M. R. Can Ultrasound Enable Efficient Intracellular Uptake of Molecules? A Retrospective Literature Review and Analysis. *Ultrasound Med. Biol.* **2012**, *38*, 876–888.
13. Lentacker, I.; De Cock, I.; Deckers, R.; De Smedt, S. C.; Moonen, C. T. W. Understanding Ultrasound Induced Sonoporation: Definitions and Underlying Mechanisms. *Adv. Drug Delivery Rev.* **2013**, 10.1016/j.addr.2013.11.008.
14. Zhang, Y.; Yu, L. C. Microinjection as a Tool of Mechanical Delivery. *Curr. Opin. Biotechnol.* **2008**, *19*, 506–510.
15. Zhong, P.; Lin, H.; Xi, X.; Zhu, S.; Bhogte, E. S. Shock Wave-Inertial Microbubble Interaction: Methodology, Physical Characterization, and Bioeffect Study. *J. Acoust. Soc. Am.* **1999**, *105*, 1997–2009.
16. Kodama, T.; Doukas, A. G.; Hamblin, M. R. Shock Wave-Mediated Molecular Delivery into Cells. *Biochim. Biophys. Acta, Mol. Cell Res.* **2002**, *1542*, 186–194.
17. Yao, C.; Qu, X.; Zhang, Z.; Hüttmann, G.; Rahmanzadeh, R. Influence of Laser Parameters on Nanoparticle-Induced Membrane Permeabilization. *J. Biomed. Opt.* **2009**, *14*, No. 054034.
18. Qin, Z.; Bischof, J. C. Thermophysical and Biological Responses of Gold Nanoparticle Laser Heating. *Chem. Soc. Rev.* **2012**, *41*, 1191–1217.

19. Pitsillides, C. M.; Joe, E. K.; Wei, X.; Anderson, R. R.; Lin, C. P. Selective Cell Targeting with Light-Absorbing Microparticles and Nanoparticles. *Biophys. J.* **2003**, *84*, 4023–4032.
20. Vivero-Escoto, J. L.; Slowing, I. I.; Wu, C.-W.; Lin, V. S. Y. Photoinduced Intracellular Controlled Release Drug Delivery in Human Cells by Gold-Capped Mesoporous Silica Nanosphere. *J. Am. Chem. Soc.* **2009**, *131*, 3462–3463.
21. Paasonen, L.; Sipilä, T.; Subrizi, A.; Laurinmäki, P.; Butcher, S. J.; Rappolt, M.; Yaghmur, A.; Urtti, A.; Yliperttula, M. Gold-Embedded Photosensitive Liposomes for Drug Delivery: Triggering Mechanism and Intracellular Release. *J. Controlled Release* **2010**, *147*, 136–143.
22. Angelos, S.; Choi, E.; Vögtle, F.; De Cola, L.; Zink, J. I. Photo-Driven Expulsion of Molecules from Mesostructured Silica Nanoparticles. *J. Phys. Chem. C* **2007**, *111*, 6589–6592.
23. Han, G.; You, C.-C.; Kim, B.-j.; Turingan, R. S.; Forbes, N. S.; Martin, C. T.; Rotello, V. M. Light-Regulated Release of DNA and Its Delivery to Nuclei by Means of Photolabile Gold Nanoparticles. *Angew. Chem., Int. Ed.* **2006**, *45*, 3165–3169.
24. El-Sayed, I. H.; Huang, X.; El-Sayed, M. A. Selective Laser Photo-Thermal Therapy of Epithelial Carcinoma Using Anti-EGFR Antibody Conjugated Gold Nanoparticles. *Cancer Lett.* **2006**, *239*, 129–135.
25. Chen, H. X.; Diebold, G. Chemical Generation of Acoustic-Waves—A Giant Photoacoustic Effect. *Science (Washington, DC, U.S.)* **1995**, *270*, 963–966.
26. Chakravarty, P.; Qian, W.; El-Sayed, M. A.; Prausnitz, M. R. Delivery of Molecules into Cells Using Carbon Nanoparticles Activated by Femtosecond Laser Pulses. *Nat. Nanotechnol.* **2010**, *5*, 607–611.
27. Halpern, B.; Benacerraf, B.; Biozzi, G. Quantitative Study of the Granulopectic Activity of the Reticulo-Endothelial System. I: The Effect of the Ingredients Present in India Ink and of Substances Affecting Blood Clotting *in Vivo* on the Fate of Carbon Particles Administered Intravenously in Rats, Mice and Rabbits. *Br. J. Exp. Pathol.* **1953**, *34*, 426–440.
28. Madsen, S. J.; Patterson, M. S.; Wilson, B. C. The Use of India Ink as an Optical Absorber in Tissue-Simulating Phantoms. *Phys. Med. Biol.* **1992**, *37*, 985–993.
29. Faraggi, E.; Gerstman, B. S.; Sun, J. Biophysical Effects of Pulsed Lasers in the Retina and Other Tissues Containing Strongly Absorbing Particles: Shockwave and Explosive Bubble Generation. *J. Biomed. Opt.* **2005**, *10*, No. 064029.
30. Leighton, T. G. In *The Acoustic Bubble*, Academic Press: 1994.
31. Prausnitz, M. R.; Lau, B. S.; Milano, C. D.; Conner, S.; Langer, R.; Weaver, J. C. A Quantitative Study of Electroporation Showing a Plateau in Net Molecular Transport. *Biophys. J.* **1993**, *65*, 414–422.
32. Oliver, J. D., III; Anderson, S.; Troy, J. L.; Brenner, B. M.; Deen, W. H. Determination of Glomerular Size-Selectivity in the Normal Rat with Ficoll. *J. Am. Soc. Nephrol.* **1992**, *3*, 214–218.
33. Escoffre, J. M.; Rols, M. P. Electrochemotherapy: Progress and Prospects. *Curr. Pharm. Des.* **2012**, *18*, 3406–3415.
34. Malietzis, G.; Monzon, L.; Hand, J.; Wasan, H.; Leen, E.; Abel, M.; Muhammad, A.; Price, P.; Abel, P. High-Intensity Focused Ultrasound: Advances in Technology and Experimental Trials Support Enhanced Utility of Focused Ultrasound Surgery in Oncology. *Br. J. Radiol.* **2013**, *86*, 20130044.
35. Stone, K. R.; Mickey, D. D.; Wunderli, H.; Mickey, G. H.; Paulsen, D. F. Isolation of a Human Prostate Carcinoma Cell Line (DU 145). *Int. J. Cancer* **1978**, *21*, 274–281.
36. Guzman, H. R.; Nguyen, D. X.; Khan, S.; Prausnitz, M. R. Ultrasound-Mediated Disruption of Cell Membranes. I. Quantification of Molecular Uptake and Cell Viability. *J. Acoust. Soc. Am.* **2001**, *110*, 588–596.
37. Schlicher, R. K.; Radhakrishna, H.; Tolentino, T. P.; Apkarian, R. P.; Zarnitsyn, V.; Prausnitz, M. R. Mechanism of Intracellular Delivery by Acoustic Cavitation. *Ultrasound Med. Biol.* **2006**, *32*, 915–924.
38. Watkins, S.; Borthwick, G.; Arthur, H. The H9c2 Cell Line and Primary Neonatal Cardiomyocyte Cells Show Similar Hypertrophic Responses *in Vitro*. *In Vitro Cell. Dev. Biol.: Anim.* **2011**, *47*, 125–131.